Egypt. J. Chem. **Vol. 67**, No. 8. pp. 157 - 169 (2024)

Egyptian Journal of Chemistry

http://ejchem.journals.ekb.eg/

Corrosion characteristics, microstructure, and mechanical properties of welding of 304SS/308LSS/304SS using GTAW.

Ahmed G. Elsayed[a], Aliaa Abdelfatah[b], Emad F. El-Kashif[a], Lamiaa Z. Mohamed[b,*], Abdallah A. Abdelkawy[a]

[a] *Department of Mechanical Design and Production in Faculty of Engineering, Cairo University, Egypt.*
[b] *Mining, Petroleum and Metallurgical Engineering Department, Faculty of Engineering, Cairo University, Egypt.*

Abstract

The gas tungsten arc welding (GTAW) method is used with different parameters to join 304SS, 308LSS, and 304SS. welding speed and gas flow rate effects on the characterization of the three welding samples were studied. Optical microscopy (OM) and scanning electron microscopy (SEM) were used to look at the base materials (BM), the heat-affected zone (HAZ), and the welding materials (WM). The tensile strength and hardness were studied for the different welding conditions. The 304SS/308LSS/304SS welding corrosion behavior was examined. The potentiodynamic polarization of the three welding conditions in 3.5% NaCl was investigated. The weld region in the low heat input sample has the lowest CR value (2.140 mm/yr), while the HAZ region in the high heat input sample has the lowest CR value (0.29 mm/yr). The SEM investigated the morphology of the three corroded welding conditions. It was found that the welding parameters had an impact on the average pit size of the corroded samples. The HAZ region in the high heat input sample has the lowest average pit size (0.329 µm).

Keywords:Welding; Tensile strength; Hardness; Corrosion behavior; Microstructure

1. Introduction

New oil reservoirs are one of the most corrosion-prone situations for metals [1, 2, 3]. Since corrosion is a major concern in the oil and gas sector, corrosion-resistant steels are constantly in demand [4, 5, 6]. These austenitic stainless steels (SS) are formable and resistant to high and cryogenic temperatures. It also resists high-temperature breaking and oxidation [7, 8]. In the oil and gas business, welding is commonly used, and the chosen procedure must assure component performance and not need excessive maintenance to maximize industrial efficiency. The breakdown or deterioration of metallic materials caused by the contact of the metal surface with the environment is known as the corrosion process [9, 10, 11, 12]. Poor SS welding procedures reduce corrosion resistance (CRST), especially stress corrosion cracking (SCC) resistance [13, 14]. Gas tungsten arc welding (GTAW) has a high arc deposition rate depending on process factors [15, 16]. A tungsten inert gas with a non-consumable electrode creates the sample arc [17, 18]. GMAW is used in various industries, including oil and gas since it produces minimal spatter and welds in all locations [1, 4]. Controlling phase balance with SS welding settings was shown [3, 4]. The GTAW has welding factors such as gas flow rate, voltage, current, polarity, welding speed, and arc duration that affect GTAW weld characteristics [19, 20, 21]. Process factors impact sample surface and mechanical characteristics [22, 23]. The bead and penetration are too tiny at high welding speeds. When the workpiece is cold, the welding speed should be lower; as it heats up, it should be faster [40]. For the same current and voltage, increasing welding speed reduces heat input

*Corresponding author e-mail: lamiaa.zaky@cu.edu.eg; (Lamiaa Z. Mohamed).
Received date 27 December 2023; revised date 29 January 2024; accepted date 04 February 2024
DOI: 10.21608/EJCHEM.2024.258625.9098

and mechanical behavior [25]. The GTAW of austenitic SS in hydrogen-argon produces stable, dependable joints with smooth surfaces. Ar shielding gas was tested with 20% hydrogen [26].

Weld tensile strength is heavily reliant on microstructure, which is influenced by welding-induced microstructural changes [18]. Industries focusing on minimizing corrosion-induced damage can consider pit size control as a factor in welding process optimization. Also, industries involving structures exposed to corrosive conditions, such as marine or chemical sectors, can implement corrosion-resistant measures based on previous studies [19]. These studies are our guide in the selection of appropriate stainless-steel grades and welding parameters for applications in chloride-rich environments [4, 5, 7]. This work aims to find out the optimum welding speed and gas flow rate effects and provides practical information for the GTAW process. Also, tensile strength and hardness under different welding conditions provide essential data on the mechanical performance of welded 304SS filled with 308LSS by using GTAW. Studying the microstructure of the base material (BM), weld material (WM), and heat-affected zone (HAZ) regions. The examination of corrosion behavior in 304SS/308LSS/304SS welds using potentiodynamic polarization (PP) in 3.5% NaCl provides insights into the electrochemical corrosion resistance of the base material (BM), weld material (WM), and heat-affected zone (HAZ) regions. Then it is investigated the welding parameters impact the average pit size of corroded welded samples in 3.5% NaCl. In the future work study these welding parameters in other media for industrial applications. These might predict mechanical failure and corrosion attack.

2. Experimental Work

The BM is SS304, and the WM is SS308L. The chemical constituents of the BM and WM are listed in Table 1. The welding was performed by GTAW bydifferent GTAW parameters were illustrated in Table 2.

Table 1 The chemical constituents of the BM (304SS) and WM (308LSS)

Materials	C	Mn	P	S	Si	Cr	Ni	Mo	Cu
304SS (BM)	0.062	1.33	0.040	0.01	0.36	18.66	9.95	0.086	0.28
308LSS (WM)	0.023	1.75	0.025	0.010	0.36	19.85	9.18	0.07	0.18

Table 2 The different GTAW parameters

Samples	welding speed, mm/min	Welding volt, V	Welding current, A	Gas flow rate, L/min
S01	41	10	84	10
S02	58	10	84	10
S03	58	12	58	15

The heat input is calculated using Eq. 1 which explains the numerical relationship between the basic parameters of welding (welding voltage, welding current, and welding speed) [27]:

$$H = \frac{V\,x\,I}{1000\,x\,S} \qquad (1)$$

Where H indicates heat input in KJ/mm, V denotes voltage in volts (V), I indicates current in amperes (A), S denotes welding speed in mm/sec.

The welded samples were cut into three regions BM, WM, and HAZ. The sample pieces were ground with SiC papers up to 1200 grit and polished using alumina paste 0.3 µm then etched. The microstructure examination was studied by optical microscopy (OM), scanning electron microscopy (SEM), and energy dispersive x-ray analysis (EDX).

The tensile examination was conducted using a 400 KN universal testing apparatus (Tinius Olsen tester Machine- model-602). Hardness profiles were measured using a load equal to 10 kg with a dwell time of 30 sec for Vickers hardness.

The polished samples of three regions BM, WM, and HAZ were characterized by potentiodynamic polarization (PP) test. The corrosion current density (i_{corr}), and corrosion potential (E_{corr}) were provided from the Tafel curves of potential vs. the logarithm of i_{corr}. The corrosion rate (CR) was calculated from Eq. (2) [28, 29] as follows:

$$CR\ (mm/Yr) = \frac{0.00327 * i_{corr} * EW.}{D} \quad (2)$$

Where i_{corr} denotes the current density in $\mu m/cm^2$, D denotes the specimen density in g/cm^3, and EW. denotes the specimen's equivalent weight in grams.

Surface morphology and composition of the three specimens after corrosion in a solution of 3.5% NaCl were investigated by SEM and EDX, respectively, for BM, HAZ, and WM.

3. Results and Discussions

3.1 Microstructure

The OM and SEM microstructures of the 304SS (BM) before weld are explored in Fig. 1. The OM image consists of austenite twins with large equiaxed grains and small amounts of ferrite grains [30]. The austenite has good CRST and low cost but produces cracks when it solidifies [31, 32]. The twin boundaries improve the mechanical properties such as strength and ductility thus 304SS is used in power plants [33, 34]. It may have some carbides in the microstructures (black spots). Fig. 2 represents the OM and SEM microstructures of 308LSS (WM) before welding with fine equiaxed austenitic grains [35]. The 308LSS has good weldability because of its low carbon content [36, 37, 38]. The Cr content is larger than 12% in 304SS and 308LSS resulting in excellent CRST because of Cr_2O_3 film formation with a high thermal expansion coefficient and less thermal conductivity [39, 40].

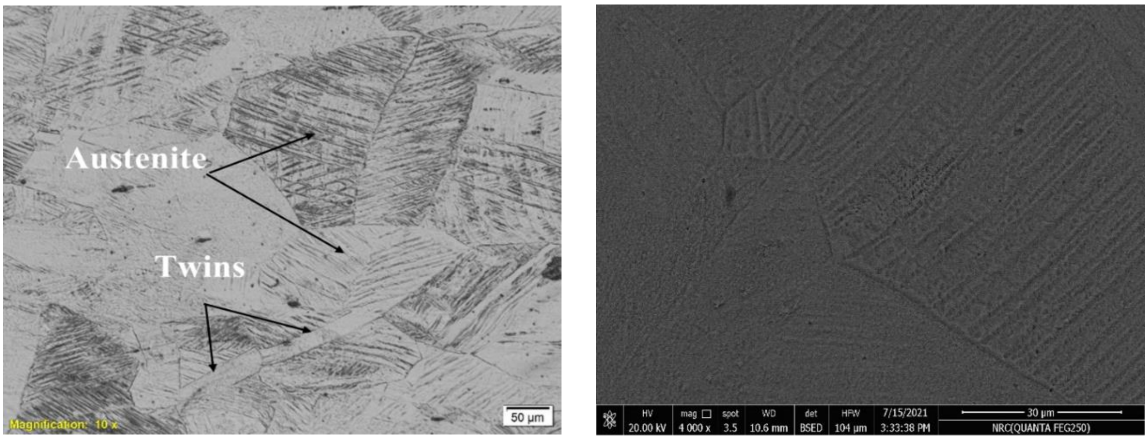

(a) (b)

Fig. 1. The microstructures of 304SS (BM) before welding (a) OM and (b) SEM

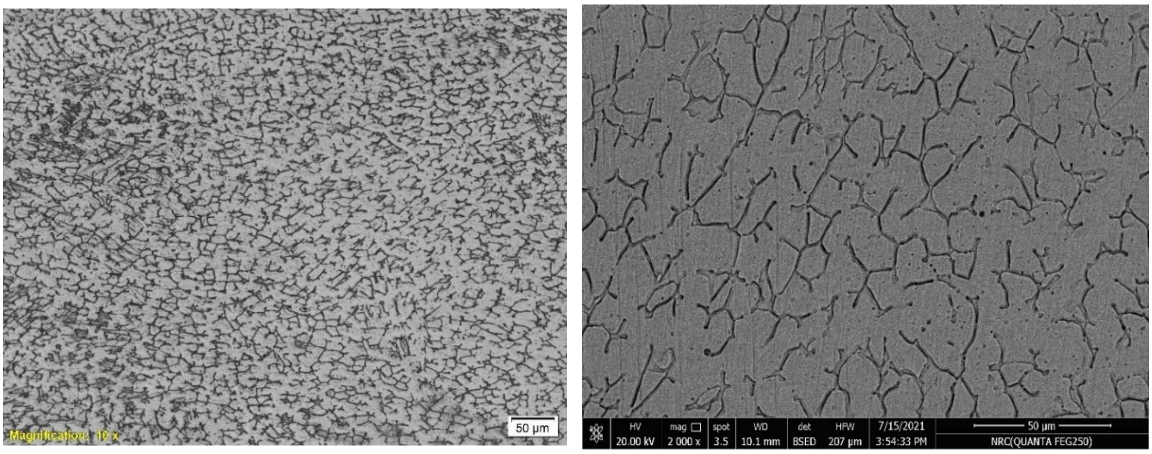

(a) (b)

Fig. 2. The microstructures of 308SS (WM) before welding (a) OM and (b) SEM

Fig. 3 represents the OM and SEM images of the three different samples after welding with different conditions of welding parameters. The welding speed has increased from 41 mm/min in S01 to 58 mm/min in S02 with the same gas flow rate where it increases from 10 L/min in S03 to 15 L/min as shown in Figs. 4 and 5. The optical microstructure of the three samples appears in the three zones (BM, HAZ, and WM) in them.

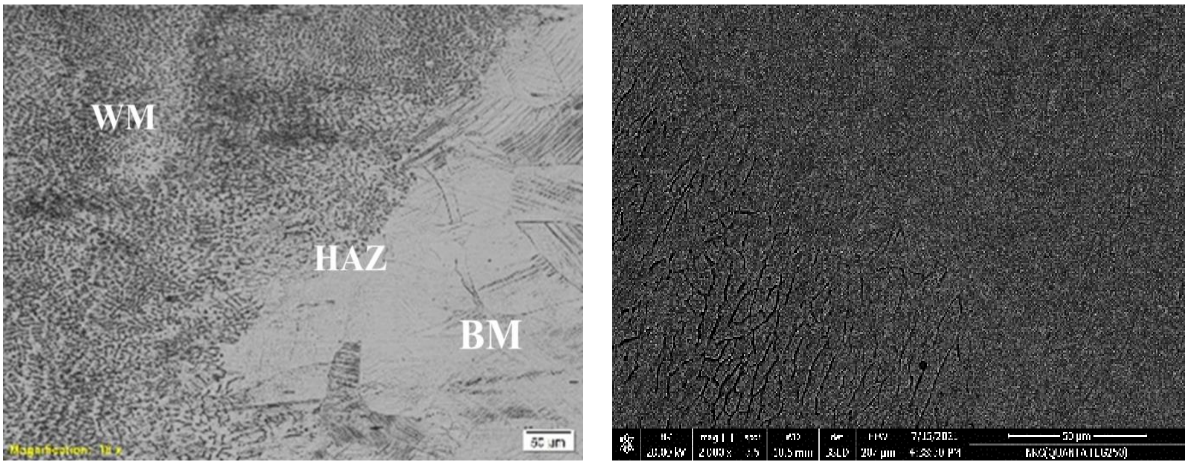

(a) (b)

Fig. 3. The microstructure of S01 sample (a) OM and (b) SEM

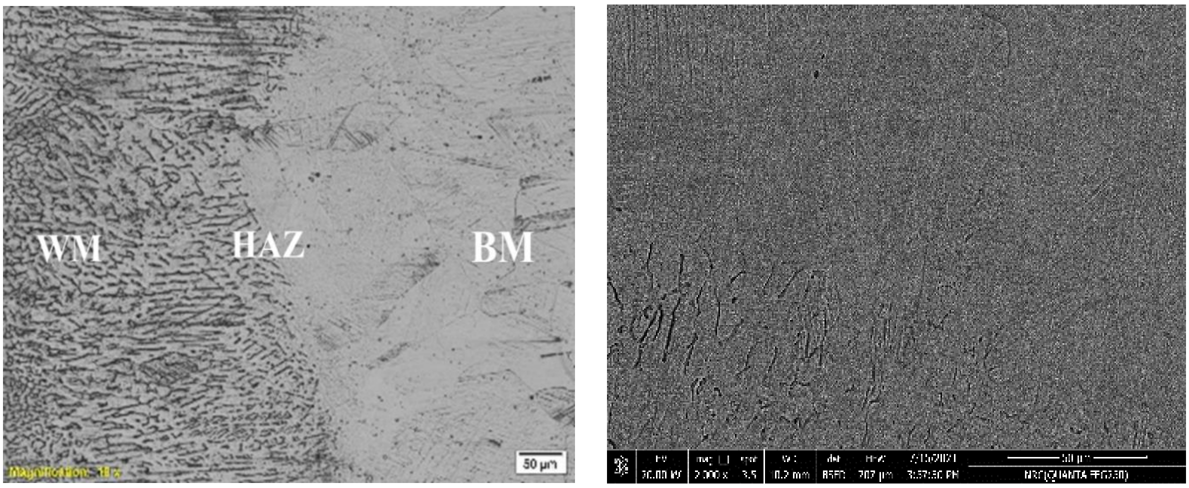

(a) (b)

Fig. 4 The microstructure of S02 sample (a) OM and (b) SEM

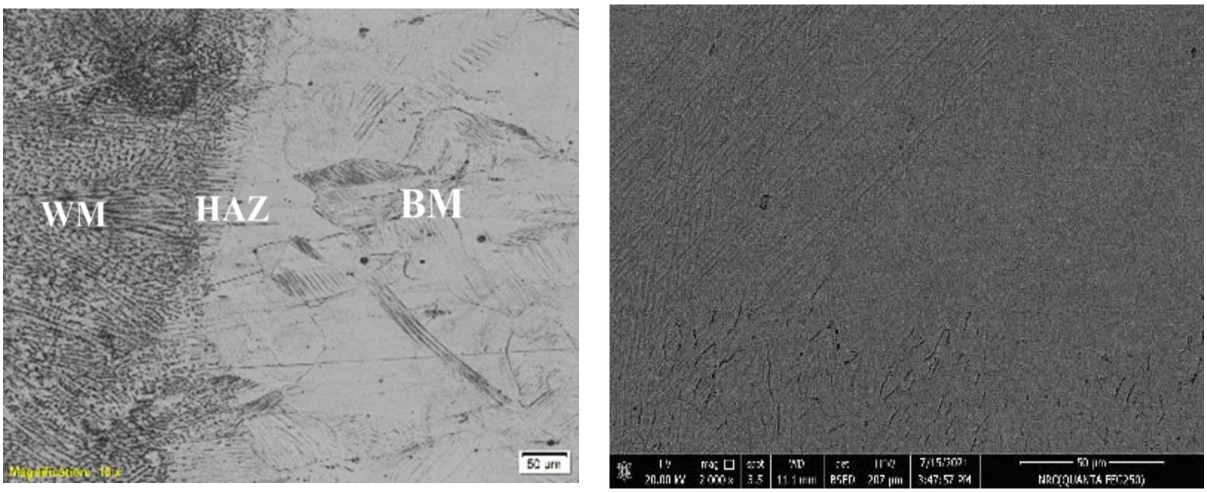

(a) (b)

Fig. 5 The microstructure of S03 sample (a) OM and (b) SEM

3.2 Tensile test

The three samples were performed to study the GTAW parameters' effect on the mechanical properties of the investigated three samples. The uniaxial tensile test of BM along with the three welded specimens using various heat input combinations was conducted to assess the joint strength at room temperature (R_T) as shown in Fig. 6 and listed in Table 3. The tensile characteristics exhibit enhancement when the heat transfer is reduced [41]. The heat input rises because the groove area or arcing parameter increases. This resulted in a significant decrease in yield strength, whereas ultimate strength remained relatively unchanged [42, 43].

Fig. 6. Welding samples of different conditions for tensile test

Table 3. Mechanical properties at significant Heat Input

Sample Number	Ultimate Tensile Strength (UTS), MPa	Yield Strength (YS), MPa	Elongation %	Heat Input KJ/cm	Remarks
BM -304SS	525	210	40.9	--	--
WM -308LSS	599	390.9	46.9	--	--
S01	591.7	362.3	39.6	8.69	Low Heat Input
S02	577.7	350.3	38.9	10.43	Medium Heat Input
S03	567.3	343.7	35.7	12.29	High Heat Input

3.3 Hardness

The hardness was estimated as a profile by Vickers hardness with 10 kg with 30 sec dwell time as seen in Fig. 7. The average hardness value of the BM is about 249 HV. The hardness of the three samples is illustrated in Fig. 7. The highest hardness is S01 which has the highest tensile strength with low heat input of the welding process. The hardness distribution in weld deposits may be because of the distribution and the size of carbide precipitation in the matrix [44].

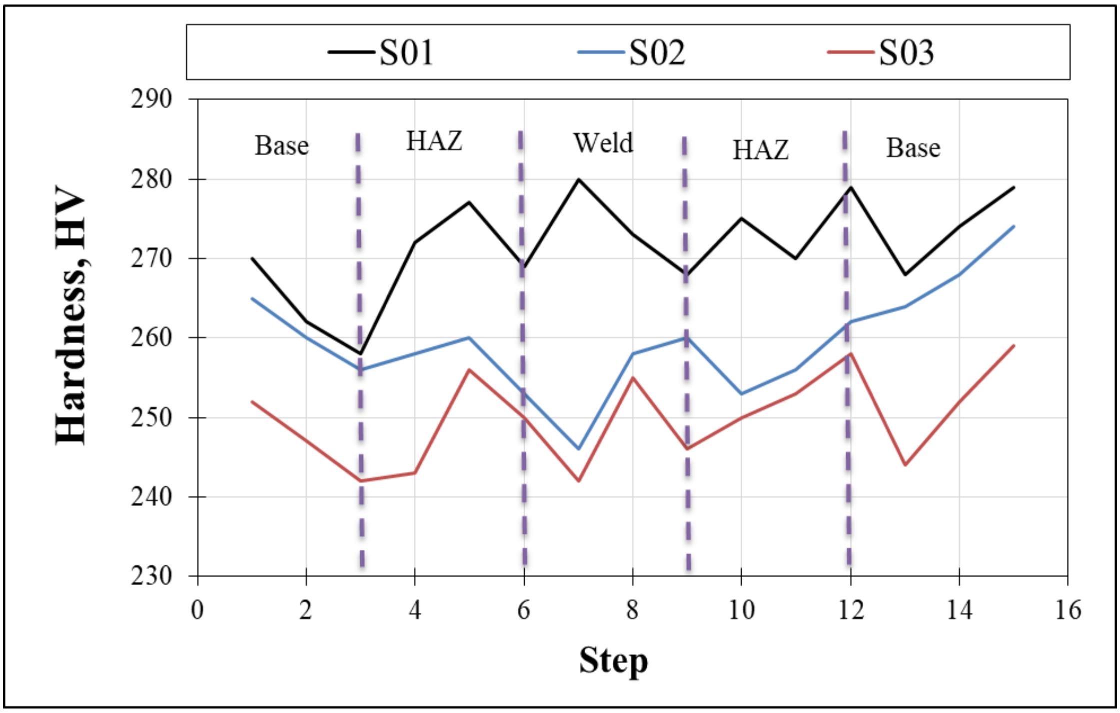

Fig. 7. Hardness of the three samples with different welding parameters

3.4 Potentiodynamic Polarization (PP)

Figs 8, 9, and 10 show the PP curves for the BM, HAZ, and WM of the three samples, respectively. From Table 4, the sample potentials range from 591.8 mV to 873.8 mV. The S01-Weld specimen has the lowest CR value (2.140 mm/yr) as compared with other conditions. The S03-HAZ specimen has the lowest CR value (0.29 mm/yr) as compared with other conditions due to the difference in average pit size as listed in Table 5. The S03-HAZ has the lowest average pit size (0.329 µm) as compared with S01-HAZ (0.513 µm) and S02-HAZ (0.726 µm).

The medium heat input results in the formation of large grain size which affects negatively hardness, strength, and CRST. The CRof S02-WM and S02-HAZ are slightly higher than S01-WM and S01-HAZ, respectively. These appear from the average pit size in Table 4 and the surface morphology after corrosion as provided in Figs.11, 12, 13, and 14. The high heat input promotes the reduction of pitting corrosion at the S03-HAZ region and crack initiation which results in lowering the CRat this region. Increasing the welding speed increases the grain size while increasing the gas flow rate leads to more fine grains, especially in the HAZ region. There is no presence of discontinuity of the welding and no phase transformation. Crack development and propagation occur in the ferrite phase of some duplex SS [45].

Increasing gas flow rate and welding speed increase the CR of WM and HAZ regions. The low-speed WM displayed the lowest electrode potential during the exposure period while the high-speed WM via verse. The electrode welding speed along the joint influences bead shape, cosmetic appearance, depth of fusion, and heat input into the BM. Faster welding speeds yield narrower beads which have less penetration. Heat input is also affected by welding speed, which in turn influences the metallurgical structure of the WM. If speeds are too fast there is a tendency for undercut, porosity, and slag inclusion, since the weld freezes quicker [46, 47].

The decrease in the CRST in SS may be explained by the well-known ‘chromium depletion theory’. For 304SS, Cr and Mo carbides precipitate along the grain boundaries (Gbs) throughout the aging. This is because the carbon diffusing is faster than Cr from the matrix to the Gbs resulting in Cr-depleted zones. The phenomenon is commonly referred to as sensitization of SS. The depleted regions are responsible for corrosion attacks but after aging time disappears of sensitization effect because of the Cr diffusion back from the matrix into the depleted zone. This phenomenon is known as healing [46, 47].

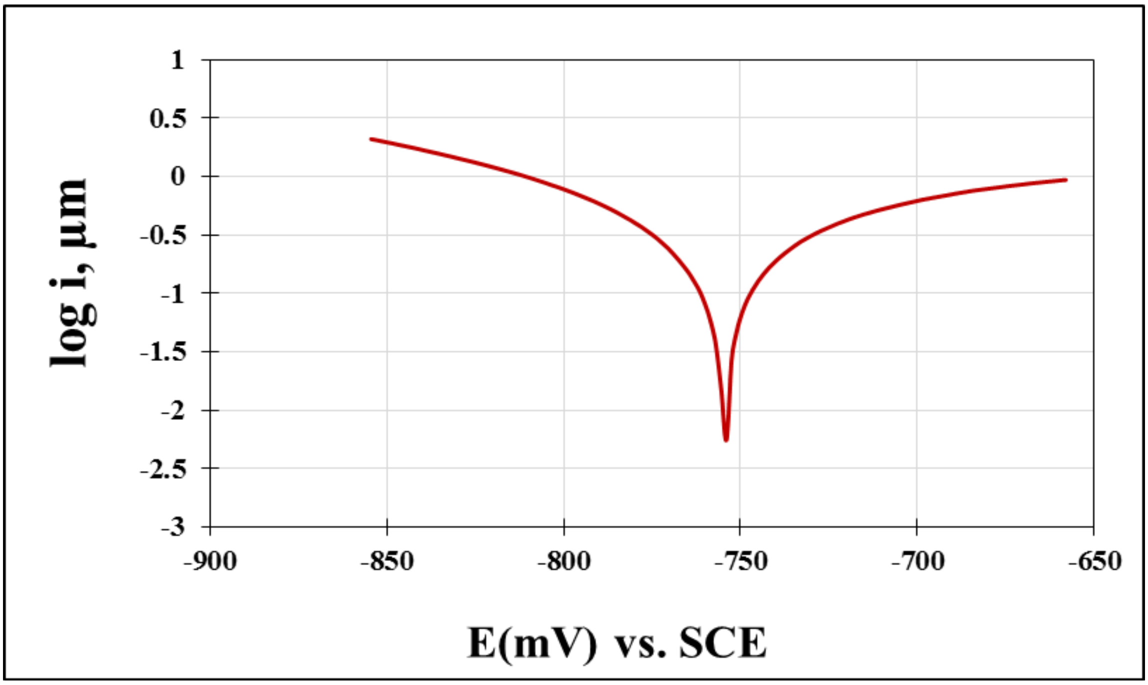

Fig. 8. The PP curve of the BM

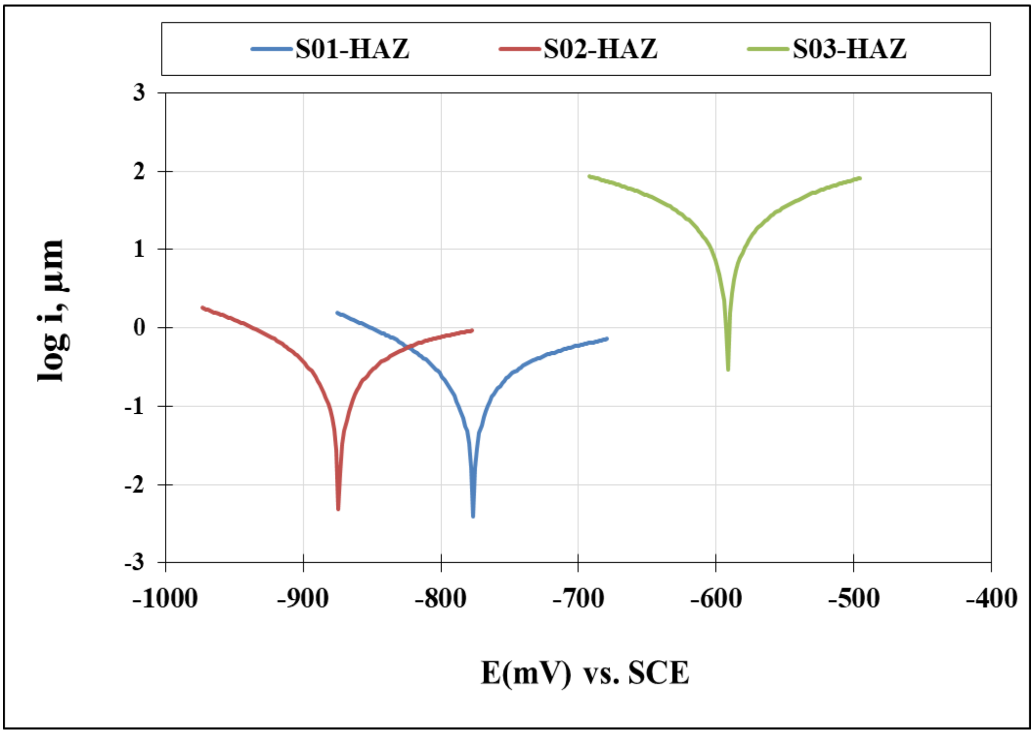

Fig. 9. The PP curves of the HAZ of the three samples

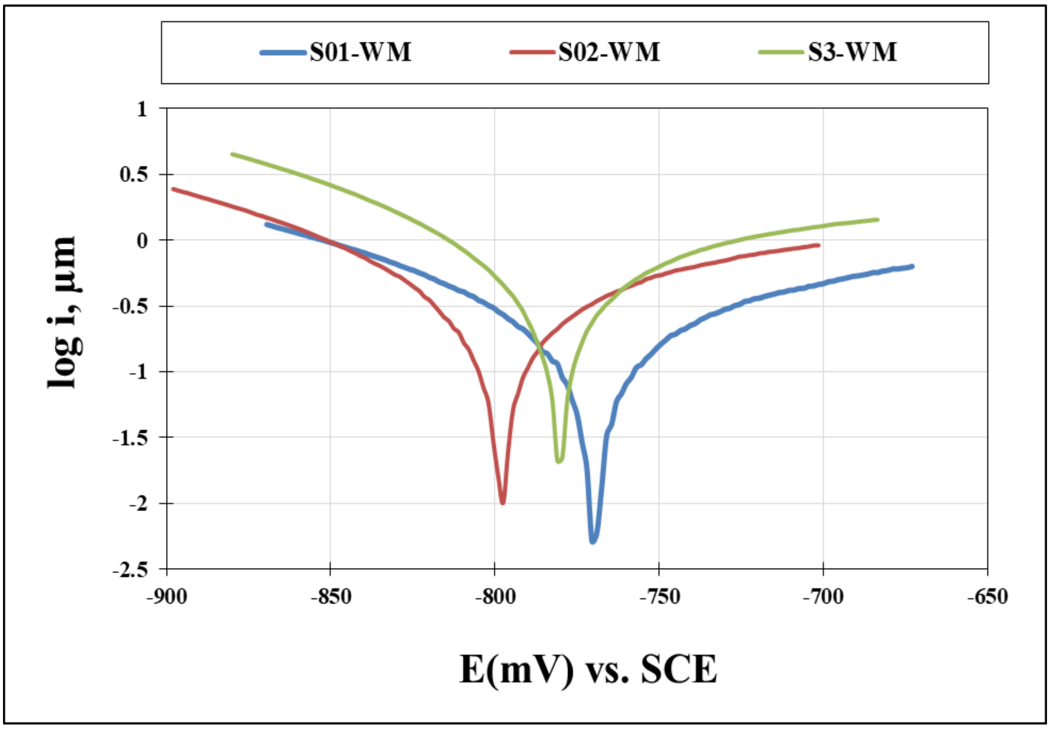

Fig. 10. The PP curves of the WM of the three samples

Table 4. The CR values of the three samples of different regions in 3.5%NaCl at R_T

Specimen	E(i=0), mV	i_{corr}, mA/cm²	Rp, ohm.cm²	CR, mm/yr
BM	-754.5	0.263	72.0	2.823
S01-HAZ	-776.6	0.230	104.6	2.471
S02-HAZ	-873.8	0.274	71.9	2.948
S03-HAZ	-591.8	0.027	1180.0	0.293
S01-WM	-769.5	0.199	120.2	2.140
S02-WM	-798.0	0.206	73.3	2.216
S03-WM	-780.5	0.494	41.7	5.308

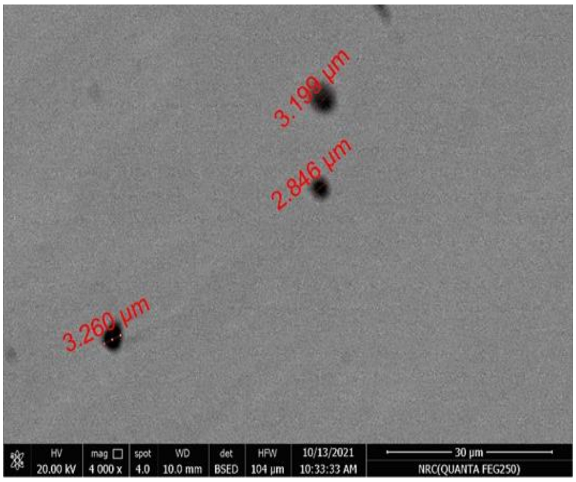

Fig. 11. The surface morphology of the corroded BM

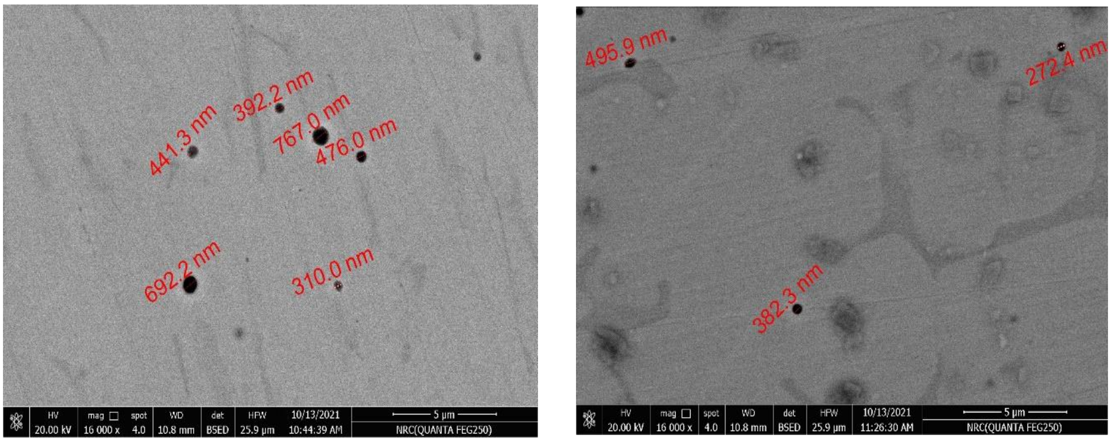

(a) (b)

Fig. 12 The surface morphology of the corroded S01 (a) HAZ, and (b) WM

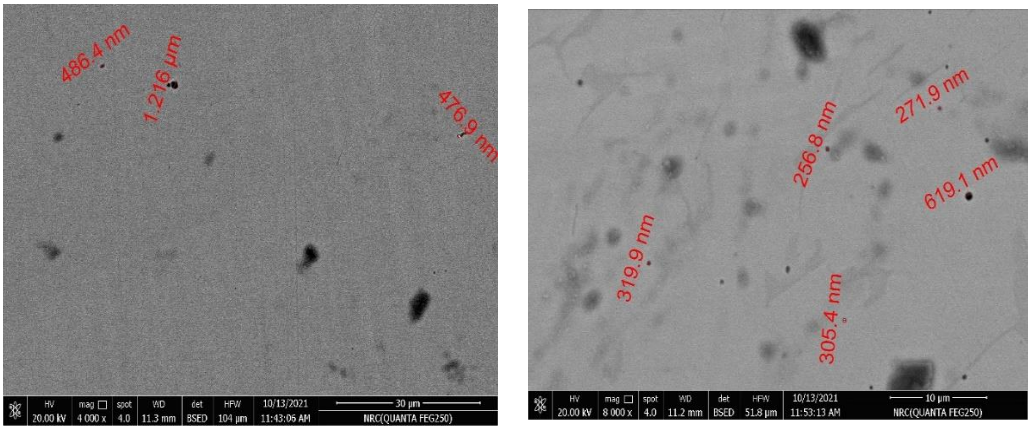

(c) (d)

Fig. 13. The surface morphology of the corroded S02 (a) HAZ, and (b) WM

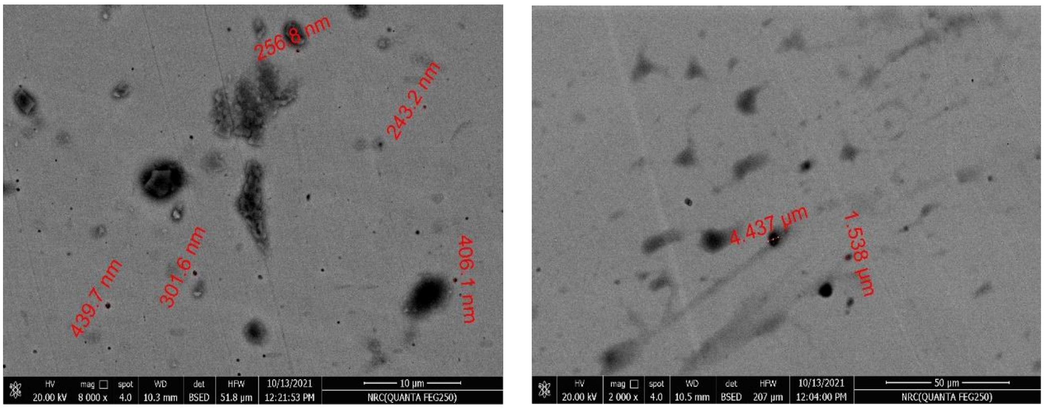

(a) (b)

Fig. 14. The surface morphology of the corroded S03 (a) HAZ, and (b) WM

Table 5. The average pit size of the three samples of different regions after corrosion in 3.5%NaCl at R_T

Specimen	Average pit size after corrosion, µm
BM	3.102
S01-HAZ	0.513
S02-HAZ	0.726
S03-HAZ	0.329
S01-WM	0.383
S02-WM	0.394
S03-WM	2.988

When welding dissimilar metals like 304SS and 308LSS using the GTAW process, the corrosion mechanism can be influenced by several factors such as electrochemical potential difference, alloying elements, HAZ, sensitization, and welding environment [48]. When two dissimilar metals are welded together, there can be a difference in their electrochemical potentials. This potential difference can lead to the formation of a galvanic couple, where one metal acts as the anode and the other as the cathode. In the case of 304SS/308LSS/304SS welding, if the potential difference between the metals is significant, it can accelerate the corrosion of the less noble metal. The composition and alloying elements present in the base metals and the filler metal (308LSS) can affect the corrosion behavior. Alloying elements, such as Cr and Ni, provide CRST to stainless steels. However, the composition and distribution of these elements in the weld zone can be affected by the welding process, potentially leading to localized corrosion [49]. During welding, the heat input can result in the formation of the HAZ adjacent to the weld. The HAZ experiences various levels of thermal cycling, which can affect the microstructure and CRST. The HAZ may contain altered grain boundaries, precipitates, and varying levels of alloying elements, potentially influencing the corrosion behavior. The welding environment can also influence the corrosion mechanism. The presence of chlorides can lead to pitting corrosion, especially if the weld is not adequately passivated or if the chloride concentration is high [50].

Stainless steels can be susceptible to sensitization, a process in which chromium carbides form along the grain boundaries, depleting the material of chromium and reducing its corrosion resistance. The heat input during welding can induce sensitization in the HAZ or the fusion zone, increasing the susceptibility to intergranular corrosion [51]. Minimizing the heat input during welding increases the CRST of weld regions and via verse in the HAZ regions due to Cr-depleted zones [46, 47]. It is important to note that the specific corrosion mechanism and behavior of the weldment can depend on the specific welding parameters, base metal conditions, and environmental factors.

Conclusions

Microstructure, mechanical, and corrosion behavior of welding of 304SS/308LSS/304SS using GTAW were investigated. It was concluded the following:

1. The microstructure was affected by the gas flow rate and welding speed of the WM and HAZ regions. Increasing the welding speed increases the grain size while increasing the gas flow rate leads to more fine grains, especially in the HAZ region. There is no presence of discontinuity of the welding and no phase transformation.
2. The highest tensile strength and hardness are obtained at low heat input during the welding. The values of tensile and hardness are satisfied according to the welding process GTAW.
3. The CRST decreases with an increase in the heat input during the welding. Also, it decreases with increasing the welding speed. Increasing the gas flow rate decreases the CRST of the WM but increases the CRST of the HAZ region.
4. The weld region in the low heat input sample has the lowest CR value (2.140 mm/yr), while the HAZ region in the high heat input sample has the lowest CR value (0.29 mm/yr).
5. Increasing the average pit size of the corroded samples in WM and HAZ regions increases the CR value. The higher heat input promotes the reduction of the pits at the HAZ region with average pit size (0.329 µm) and cracks initiations that decrease the CR value at this region.

Declaration of Competing Interest

There are no conflicts to declare.

References

1. M.A. Alsahlawi, The future prospect of world oil supply: Depletion of resources or price trends. OPEC Energy Rev. 2009, 34, 73–81.
2. C. Campbell, World Oil: Reserves, Production, Politics and Prices, 1st ed.; Dore, A., Sinding-Larsen, R., Eds.; Norwegian Petroleum Society Special Publications: Norwegian, Norway, 6, 1996.
3. S. Chacón-Fernández, A. Portolés-García, G. Romgvaní-Labanda, Analysis of the influence of GMAW process parameters on the properties and microstructure of S32001 steel. Materials 2022, 15, 6498.
4. A. F. Miranda-Pérez, B. R. Rodríguez-Vargas, I. Calliari, L. Pezzato, Corrosion Resistance of GMAW Duplex Stainless Steels Welds, Materials 2023, 16, 1847.
5. A. Eghlimi, M. Shamanian, M. Eskandarian, A. Zabolian, J.A. Szpunar, Characterization of microstructure and texture across dissimilar super duplex/austenitic stainless steel weldment joint by super duplex filler metal. Mater. Charact. 2015, 106, 27–35.
6. Hou, Y.; Nakamori, Y.; Kadoi, K.; Inoue, H.; Baba, H. Initiation mechanism of pitting corrosion in weld heat affected zone of duplex stainless steel. Corros. Sci. 2022, 201, 110278.
7. Y. Hu, Y. Shi, X. Shen, Z. Wang, Microstructure, pitting corrosion resistance and impact toughness of duplex stainless steel underwater dry hyperbaric flux-cored arc welds. Materials 2017, 10, 1443.
8. J.C. Lippold, D.J. Kotecki, Welding Metallurgy and Weldability of Stainless Steels, 1st ed.;

John Wiley & Sons, Inc.: Hoboken, NJ, USA, 2005.

9. A. M. El-Shamy, Y. Reda, K. M. Zohdy, A.K. Eessaad, Effect of Plating Materials on the Corrosion Properties of Steel Alloy 4130, Egypt. J. Chem. 63(2), 579-597 (2020)
10. M.M. Megahed, M.Y. Sedeka, A.M. El-Shamy, Selective Formula as a Corrosion Inhibitor to Protect the Surfaces of Antiquities Made of Leather-Composite Brass Alloy, Egypt. J. Chem. Vol. 63, No. 12 pp. 5269 - 5287 (2020)
11. A. M. El-Shamy, M. Abdelbar, Ionic Liquid as Water Soluble and Potential Inhibitor for Corrosion and Microbial Corrosion for Iron Artifacts, Egypt. J. Chem. Vol. 64, No. 4 pp. 1867 - 1876 (2021)
12. M.M. Megahed, M.M. Abdelbar, E.M. Abouelez, A.M. El-Shamy, Polyamide Coating as a Potential Protective Layer Against Corrosion of Iron Artifacts, Egypt. J. Chem. Vol. 64, No 10 pp. 5693 – 5702 (2021)
13. S. Kumar, A.S. Shahi, Effect of heat input on the microstructure and mechanical properties of gas tungsten arc welded AISI 304 stainless steel joints. Mater. Des. 2011, 32, 3617–3623.
14. V. Linton, N. Laycock, S Thomsen, A. Klumpers, Failure of a super duplex stainless steel reaction vessel. Eng. Fail. Anal. 2004, 11, 1350–6307.
15. X. Miao, H. Zhang, F. Ge, Z. He, J. Gao, Z. Su, Research on Arc Morphology and Keyhole Behavior of Molten Pool in Magnetically Controlled Plasma-GMAW Welding, Metals 2023, 13, 148
16. J. Vora, N. Parikh, R. Chaudhari, V. K. Patel, H. Paramar, D. Y. Pimenov, K. Giasin, Optimization of Bead Morphology for GMAW-Based Wire-ArcAdditive Manufacturing of 2.25 Cr-1.0 Mo Steel Using Metal-Cored Wires, Appl. Sci. 2022, 12, 5060
17. S. S. Karganroudi, M. Moradi, M. A. Attar, S. A. Rasouli, M. Ghoreishi, J. Lawrence, H. Ibrahim, Experimental and Numerical Analysis on TIG Arc Welding of Stainless Steel Using RSM Approach. Metals 2021, 11, 1659.
18. K. Kornokar, F. Nematzadeh, H. Mostaan, A. Sadeghian, M. Moradi, D. G. Waugh, M. Bodaghi, Influence of Heat Input on Microstructure and Mechanical Properties of Gas Tungsten Arc Welded HSLA S500MC Steel Joints, Metals 2022, 12, 565.
19. A. G. Elsayed, A. A. Abdelkawy, E. F. El-Kashif, The Influence of GTAW Parameters on Microstructure and Mechanical Behaviour of Austenitic Weldments—A review, International Journal of Scientific & Engineering Research, 8(1), 2017
20. Q. Ma, C. Luo, S. Liu, H. Li, P. Wang, D. Liu, Y. Lei, Investigation of arc stability, microstructure evolution and corrosion resistance in underwater wet FCAW of duplex stainless steel. J. Mater. Res. Technol. 2021, 15, 5482–5495.
21. E. Montero-Monsalvo, J.S. Mora-Flores, M.A. Martínez-Damián, M. Hernández-Juárez, R. Valdivia-Alcalá, Oil and gasoline market analysis in Mexico. Agrociencia 2018, 52, 1179–1193.
22. A. Kumar, K. Maji, Selection of process parameters for near-net shape deposition in wire arc additive manufacturing by genetic algorithm. J. Mater. Eng. Perform. 2020, 29, 3334–3352.
23. T. d. V. Tomaz, F.H.G. Colaço, S. Sarfraz, D.Y. Pimenov, M. K. Gupta, G. Pintaude, Investigations on quality characteristics in gas tungsten arc welding process using artificial neural network integrated with genetic algorithm. Int. J. Adv. Manuf. Technol. 2021, 113, 3569–3583.
24. S. Helzer, H. Cary, Modern welding technology. 6th Ed. Upper Saddle River (NJ): Pearson Education, Inc.; 2005
25. B.Kutelu B, Seidu S, Eghabor G, et al. review of GTAW welding parameters. J Miner Mater Charact Eng. 2018; 6: 541–554.
26. J. Tusek, M. Suban, Experimental research of the effect of hydrogen in argon as a shielding gas in arc welding of high-alloy stainless steel. Int J Hydrog Energy. 2000; 25:369–376
27. R. W. Niles, C. E. Jackson, Weld thermal efficiency of the GTAW process. Weld. J. 1975, 54, 25
28. S. Elkatatny, L.Z. Mohamed, W. Abd-Elaziem, A. Abdelfatah, Corrosion resistance of nonequiatomicFeNiCrMnAlx high entropy alloys in hexamine as inhibitor in 3.5% NaCl, Materials and Corrosion, 2024
29. H. Abd El-Fattah, L.Z. Mohamed, I. Elmahallawi, A. Abdelfatah, Corrosion characteristics of Ti and Al2O3/Ti thin films sputtered on 316LSS, International Journal of Electrochemical Science 19 (2024) 100426
30. C. Pandey, Mechanical and Metallurgical Characterization of Dissimilar P92/SS304 L Welded Joints Under Varying Heat Treatment Regimes, Metall. Mater. Trans. A, 51(5), 2126–2142, 2020.
31. R.K. Buddu, N. Chauhan, P.M. Raole, H. Natu, Studies on Mechanical Properties, Microstructure and Fracture Morphology

Details of Laser Beam Welded Thick SS304 L Plates for Fusion Reactor Applications, Fusion Eng. Des., 95, pp. 34–43, 2015.

32. D. K. Singh, G. Sahoo, R. Basu, V. Sharma, M.A. Mohtadi-Bonab, Investigation on the Microstructure—Mechanical Property Correlation in Dissimilar Steel Welds of Stainless-Steel SS 304 and Medium Carbon Steel EN 8, J. Manuf. Process., 36, 281–292, 2018.
33. A.Y. Chen, W.F. Hu, D. Wang, Y.K. Zhu, P. Wang, J.H. Yang, X.Y. Wang, J.F. Gu, J. Lu, Improving the Intergranular Corrosion Resistance of Austenitic Stainless Steel by High Density Twinned Structure, Scr. Mater., 130, 264–268, 2017.
34. K. Chandra, V. Kain, P. Ganesh, Controlling End-Grain Corrosion of Austenitic Stainless Steels," J. Mater. Eng. Perform., 17(1), 115–122, 2008.
35. A. Mortezaie, M. Shamanian, An Assessment of Microstructure, Mechanical Properties and Corrosion Resistance of Dissimilar Welds Between Inconel 718 and 310S Austenitic Stainless Steel, Int. J. Pressure Vessels Piping, 116, 37–46, 2014.
36. L. Boriwal, R.M. Sarviya, M.M. Mahapatra, Optimization of Weld Bonding Process Parameters of Austenitic Stainless Steel 304 L and Low Carbon Steel Sheet Dissimilar Joints," J. Adhes. Sci. Technol., 31(14), 1591–1616, 2017.
37. M. Shakil, M. Ahmad, N.H. Tariq, B.A. Hasan, J.I. Akhter, E. Ahmed, M. Mehmood, M.A. Choudhry, M. Iqbal, Microstructure and Hardness Studies of Electron Beam Welded Inconel 625 and Stainless Steel 304 L, Vacuum, 110, 121–126, 2014.
38. N. Kumar, C. Pandey, P. Kumar, Dissimilar Welding of Inconel Alloys With Austenitic Stainless-Steel: A Review, Journal of Pressure Vessel Technology, 145, 011506-1, 2023
39. J.A. Siefert, S.A. David, J.A. Siefert, S.A. David, Weldability and Weld Performance of Candidate Austenitic Alloys for Advanced Ultrasupercritical Fossil Power Plants, Sci. Technol. Weld. Joining, 19(4), 271–294, 2014.
40. Z. Zhang, Z.F. Hu, L.F. Zhang, K. Chen, P.M. Singh, Effect of Temperature and Dissolved Oxygen on Stress Corrosion Cracking Behavior of P92 Ferritic-Martensitic Steel in Supercritical Water Environment, J. Nucl. Mater., 498, 89–102, 2018.
41. S. Kumar, N. A. Barla, R. Anant, K. K. Saxena, A study on shrinkage residual stresses, microstructure and mechanical properties of ASS thick pipe welded by GMAW process, Mater. Res. Express 8 (2021) 116504
42. S.G. Kulkarni, P.K. Ghosh, Improvement of weld characteristics by variation in welding processes and parameter in joining of thick wall 304LN stainless steel pipe, ISIJ Int., 48 1560–9, 2008
43. R. Kumar, P.K. Ghosh, S. Kumar, Thermal and metallurgical characteristics of surface modification of AISI 8620 steel produced by TIG arcing process J. Mater. Process. Technol. 240 420–31, 2017
44. A. Joseph, D. Harwig, D.F. Farson, R. Richardson, Measurement and calculation of arc power and heat transfer efficiency in pulsed gas metal arc welding Sci. Technol. Weld. Joining 8 400–6, 2003
45. J.O. Nilsson, A. Wilson, Influence of Isothermal Phase Transformations on Toughness and Pitting Corrosion of Super Duplex Stainless Steel SAF 2507. Mater. Sci. Technol. 1993, 9, 545–554.
46. A. N. Kamel, E. R. Elsharkawy, A. F. Waheed, Effect of Aggressive Media on the Corrosion Behavior Dissimilar, Welding of 308L Stainless Steels Deposited on Carbon Steel, American Journal of Engineering Research (AJER), 8(6), 184-191, 2019
47. C.V. Robino, M. J. Cieslak, P. W. Hochanadel, G. R. Edwards, Heat treatment of investment cast PH 13-8 Mo stainless steel: Part II. Isothermal aging kinetics, Metallurgical and Materials Transactions A, 25(4) (1994) 697-704.
48. A. Mitru, A. Semenescu, G. Simion, E. Scutelnicu, I. Voiculescu, Study on the Weldability of Copper—304L Stainless Steel Dissimilar Joint Performed by Robotic Gas Tungsten Arc Welding, Materials 2022, 15, 5535
49. G.R. Mohammed, M. Ishak, S.N. Aqida, H.A. Abdulhadi, Effects of Heat Input on Microstructure, Corrosion and Mechanical Characteristics of Welded Austenitic and Duplex Stainless Steels: A Review, Metals 2017, 7, 39
50. Y. Xie, S. Guo, A. Leong, J. Zhang, Y. Zhu, Corrosion behaviour of stainless steel exposed to highly concentrated chloride solutions, Corros. Eng. Sci. Telchnol. 52(4), 283–293, 2017.
51. A.C. Gonzagaa, C. Barbosa, S.S.M. Tavares, A. Zeemann, J.C. Payão, Influence of post welding heat treatments on sensitization of AISI 347 stainless steel welded joints, J. Mater. Res. Technol., 9(1), 2020, 908-921